Available online at www.sciencedirect.com
ScienceDirect
Journal of Solid State Chemistry 181 (2008) 190–198
JOURNAL OF SOLID STATE CHEMISTRY
www.elsevier.com/locate/jssc

$ScRe_2O_6$: A new ternary oxide with metallic Re–Re-bonds and a ferromagnetic component above room temperature

D. Mikhailova[a,b,*], H. Ehrenberg[a,b], G. Miehe[a], D. Trots[a], C. Hess[b], R. Schneider[b], H. Fuess[a]

[a]*Institute for Materials Science, Darmstadt University of Technology, D-64287, Darmstadt, Germany*
[b]*IFW Dresden, Helmholtzstr. 20, D-01069 Dresden, Germany*

Received 2 August 2007; received in revised form 2 November 2007; accepted 10 November 2007
Available online 22 November 2007

Abstact

A new phase in the system Sc–Re–O, $ScRe_2O_6$, was synthesized for the first time in sealed silica tubes and its crystal structure was solved by single crystal X-ray diffraction. $ScRe_2O_6$ (space group $P2_1/a$, $a = 5.6176(9)$ Å, $b = 4.7970(9)$ Å, $c = 7.5143(16)$ Å, $\beta = 97.49(2)^\circ$, $Z = 2$) crystallizes in a new rutile-type structure, derived from three formula units by splitting the cation site in ratio 1:2. Re_2O_{10} clusters can be considered as structural units, in which the rhenium ions form pairs by metallic bonds with a Re–Re distance of 2.523(3) Å. No phase transition was observed in the temperature range of 295–930 K. The compound has a metallic character of conductivity in the temperature range of at least 4–950 K and displays a ferromagnetic ordering above room temperature (''unconventional Re-magnetism'').

PACS: 61.66.Fn

Keywords: $ScRe_2O6$; Rutile-like structure; Cations ordering; Re_2O_{10}-clusters; Re–Re metallic bond; Ferromagnetism of Re(+4.5)

1. Introduction

A distinguishing feature of all ternary oxides of Sc and heavy transition *d*-elements such as Hf, Ta or W, is the highest oxidation state of the heavy *d*-metal and, therefore, the absence of metallic bonding in the structure. M_7O_{12}, M_7O_{13}, $M_7O_{11.5}$ and M_9O_{17}, where M is Sc and a 5*d*-metal in different ratios, depending on the oxidation state of the 5*d* element, represent the largest class of compounds with the same structure type [1–4]. They crystallize in a rhombohedral fluorite-like structure (S.G. *R*-3) with oxygen vacancies, in which the heavy *d*-elements occupy a Wyckoff (3*a*) site with higher local symmetry and randomly share a Wyckoff (18*f*) site with Sc atoms. Oxygen atoms around metal atoms form polyhedra (MO_6, MO_7 or MO_8), connected via edges and corners. Some M_7O_{12} phases undergo a thermally or irradiation-induced rhombohedral-to-cubic order–disorder phase transition [3]. The compounds $ScMO_4$ with $M = Nb$, Ta crystallize at ambient conditions in wolframite-type structures [2,4,5] and demonstrate a phase transition from paraelectric to ferroelectric [5]. In the Sc–*M*–O system, where $M = Mo$ or W, two isostructural compounds, $Sc_2(MoO_4)_3$ and $Sc_2(WO_4)_3$ exist [2]. Little information is reported on the Sc–Re–O system, although different oxidation states of Re offer a rich variety of compositions with different Sc/Re ratios and different crystal structure types. The study of this system can also contribute to investigations of ''pure'' Re-magnetism in ternary oxides, because the Sc^{3+} ion is diamagnetic. Sc_6ReO_{12} (M_7O_{12}) is an example of a Sc,Re-compound with Re^{+6} [6]. It adopts a rhombohedral fluorite-like structure (S.G. *R*-3) as well as Sc_6WO_{12} [2,7] or Ln_6ReO_{12} (Ln = Ho, Er, Tm, Yb and Lu) [8], shows a maximum of magnetization at 1.89 K and a magnetic moment per Re^{+6} ion of 0.65 μ_B. For Re^{+7}, the perrhenate $Sc(ReO_4)_3$ [9] is known, but the crystal structure was determined only for the trihydrate $Sc(ReO_4)_3 \cdot 3H_2O$

*Corresponding author at: Institute for Materials Science, Darmstadt University of Technology, D-64287, Darmstadt, Germany.
Fax: +49 6151 16 6023.
E-mail address: mikhailova@st.tu-darmstadt.de (D. Mikhailova).

0022-4596/$ - see front matter © 2007 Elsevier Inc. All rights reserved.
doi:10.1016/j.jssc.2007.11.021

[10]. In this work we report synthesis, crystal structure and the investigation of some physical–chemical properties of a new phase formed in the ternary Sc–Re–O system: $ScRe_2O_6$.

2. Experimental

2.1. Two-temperature synthesis of $ScRe_2O_6$ in sealed silica tubes

The starting materials used were Sc_2O_3 (Strem Chemicals, 99.99%), ReO_2 (Alfa Aesar, 99.99%) and ReO_3 (Strem Chemicals, 99.9%). Before use, the oxides were dried in air at 110–115 °C for 2–3 h. The oxides (about 1 g of total mass) were weighed with the accuracy of 0.0005 g, ground together in an agate mortar under acetone and pressed into pellets. Two such pellets of an Sc_2O_3, ReO_2 and ReO_3 mixture in two Al_2O_3 or quartz crucibles were separated from each other by a small quartz stick and placed in a silica tube. The tube was evacuated and placed into a tube furnace with a 20–30 °C temperature gradient. The synthesis temperature was 1223 K. After 30–33 h, the sealed tubes were quenched from the synthesis temperature in air.

2.2. High-pressure high-temperature synthesis of $ScRe_2O_6$

A high-pressure synthesis of $ScRe_2O_6$ was performed in a Girdle–Belt apparatus with pyrophyllite as the pressure-transmitting medium. A graphite furnace and a platinum capsule containing the reactants were used for the experiment. A mixture of Sc_2O_3 (Strem Chemicals, 99.99%) and ReO_3 (Strem Chemicals, 99.9%) in molar ratio Sc:Re = 2:3 was ground in an agate mortar under acetone and filled into a platinum capsule. The sample holder was pressed up to 5 GPa before the temperature was raised to 1350 °C with a rate of 50°/min. The heating current was switched off after 120 min and after cooling to room temperature, pressure was released.

2.3. X-ray powder diffraction (XPD)

Phase analysis, determination of cell parameters and preliminary structure solution were based on X-ray powder diffraction data, collected with a STOE STADI P diffractometer (Mo $K\alpha_1$-radiation, $\lambda = 0.7093$ Å) in transmission mode. All diffraction patterns have been analyzed by full-profile Rietveld refinements, using the software package WinPLOTR [11].

2.4. Single-crystal X-ray diffraction

The crystal structure of $ScRe_2O_6$ was solved based on single-crystal X-ray diffraction data, measured with an Xcalibur system from Oxford Diffraction. The software packages SHELXS [12] and SHELXL [13] were used for structure solution and refinement as included in X-STEP32 [14]. A combined empirical absorption correction with frame scaling was applied, using the scale3 abspack command in CrysalisRed [15].

2.5. X-ray synchrotron diffraction

A high-temperature structural investigation on an $ScRe_2O_6$ powder has been performed over the temperature range of 293–930 K by X-ray synchrotron diffraction at HASYLAB/DESY (Hamburg, Germany) at beam-line B2. A 0.3 mm quartz capillary was filled with powdered $ScRe_2O_6$ in the glove-box under Ar-atmosphere, sealed and mounted inside a STOE furnace in Debye–Scherrer geometry, equipped with a EUROTHERM temperature controller and a capillary spinner. The data were collected in steps of 0.004° for the 2θ range from 4° to 40° in temperature steps of 100 K. The wavelength of 0.49962(1) Å was determined from eight reflection positions of a LaB_6 reference material. After heating up to 930 K and following cooling, the $ScRe_2O_6$ sample was analyzed again at room temperature.

All diffraction patterns have been analyzed using the software package WinPLOTR [11]. For the structure model, a full-profile Rietveld refinement of the oxygen and rhenium positions was performed with an isotropic approximation for the thermal displacement parameters, which were refined constrained for all oxygen atoms and independently for the Sc and Re sites.

2.6. Electron diffraction

The electron diffraction investigations were performed on a Philips CM20 transmission electron microscope, operating at an accelerating voltage of 200 kV. On-line cell parameter determinations were made using the software program package Program for Interpreting Electron diffraction Patterns (PIEP) [16].

2.7. EPMA

A quantitative determination of the Sc and Re contents in the $ScRe_2O_6$ sample was carried out by electron probe microanalysis (EPMA) with a JEOL JXA-8900 R Superprobe using an accelerating voltage of 15 kV, a beam current of 80 nA and a 3 μm measuring spot. The total volume analyzed is around 10–15 μm^3.

2.8. Differential thermal analysis (DTA–TG)

A simultaneous thermal analyzer NETZSCH STA 429 (CD) operated with dry and purified Ar was used to register mass loss and thermal flux curves. About 30 mg of $ScRe_2O_6$ were heated in an Al_2O_3-crucible with a rate of 5 K/min from 293 to 1373 K.

2.9. Magnetic behavior

The magnetic properties of $ScRe_2O_6$ have been studied with a superconducting quantum interference device (SQUID) from Quantum Design. Measurements were performed upon heating in field cooled and zero-field cooled mode over the temperature range from 1.8 to 350 K and at constant temperature in field strengths up to 5.5 T.

2.10. Resistivity measurements

Low-temperature resistivity of an $ScRe_2O_6$ pellet with 4 mm^2 surface area was measured by the standard four-probe method in the temperature range of 4–270 K. Copper wires were attached to the sample using EPOTEC H20E silver epoxy, and the contacts were annealed at 673 K for 15 min in air.

3. Results

3.1. Two-temperature synthesis of $ScRe_2O_6$ in a sealed silica tube and sample characterization

A synthesis of $ScRe_2O_6$ with fixed Re_2O_7 pressure in the reaction tube was performed by the two-temperature synthesis as described in Ref. [6] for the synthesis of Sc_6ReO_{12}. At higher temperature in a gradient furnace (T_1, 1243–1253 K) a mixture of Sc_2O_3, ReO_2 and $ScRe_2O_6$, which was formed during the synthesis, was used to adjust the Re_2O_7 partial pressure in the tube, whereas at the lower temperature T_2 (1223 K), single-phase $ScRe_2O_6$ formed [6]. Our preliminary experiments have shown that the Re_2O_7 pressure inside the silica tube during the synthesis at 1223 K (the temperature of the second pellet was 1243 K) can reach 0.3–0.4 atm. For this estimation, pellets of the reacting mixture were weighed before the synthesis and after quenching the tube into water from synthesis temperature. It is assumed that the mass difference of the pellet corresponds to Re_2O_7 evaporation. Phase composition of both pellets was always confirmed by X-ray diffraction.

The diffraction pattern of the $ScRe_2O_6$ phase, which was obtained by the two-temperature synthesis, is presented in Fig. 1. All reflections were explained based on a monoclinic unit cell with lattice parameters $a = 5.6144(2)$ Å, $b = 4.7906(1)$ Å, $c = 7.5187(2)$ Å and $\beta = 97.601(2)^\circ$.

The EPMA measurements performed on two to three spots on five to six grains of $ScRe_2O_6$ have shown that the average Sc:Re ratio is 1:2 within 2% of relative uncertainty.

According to the DTA of $ScRe_2O_6$ performed in Ar-atmosphere, the compound decomposes in two steps (Fig. 2), which was also confirmed by X-ray diffraction. The first mass loss observed at a temperature of about 936 K corresponds to the following reaction:

$$6ScRe_2O_6 \Leftrightarrow 3Sc_2O_3(s) + 10ReO_2(s) + Re_2O_7(g). \quad (1)$$

It was confirmed by X-ray diffraction of an $ScRe_2O_6$ sample, which was also annealed in Ar-atmosphere at 953 K. The measured mass loss (15.53%) is in a very good agreement with the theoretical value (15.73%) for reaction (1). The second step of mass loss was at 1257 K and corresponds to the disproportionation of ReO_2:

$$7ReO_2(s) \Leftrightarrow 3Re(s) + 2Re_2O_7(g). \quad (2)$$

The difference between the measured mass loss in the second step and the theoretical one is about 2%. The residue after the analysis contained only Sc_2O_3 and Re, according to X-ray diffraction, as expected.

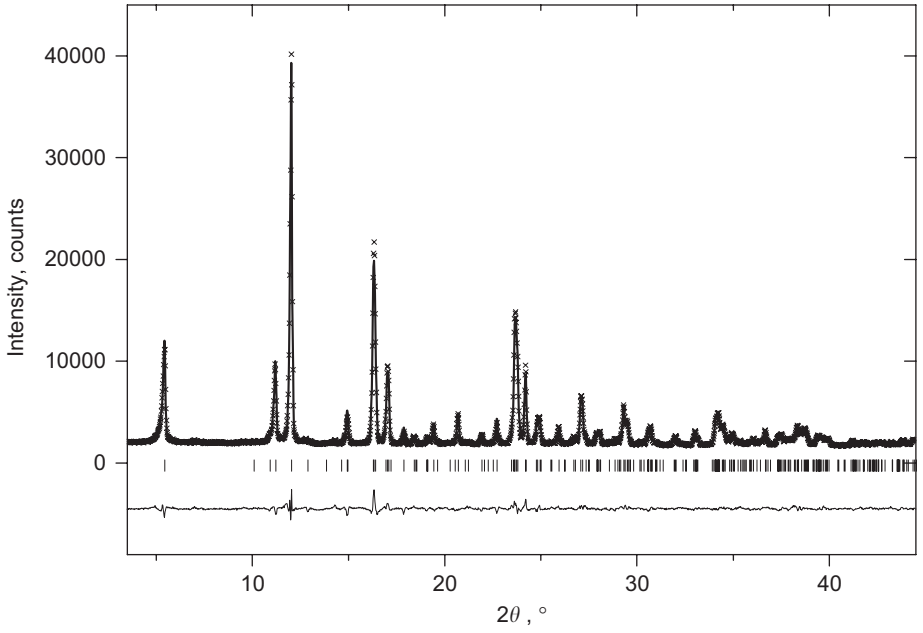

Fig. 1. The observed and fitted profiles together with the corresponding difference curve (Mo $K\alpha_1$) for $ScRe_2O_6$, obtained by a two-temperature synthesis.

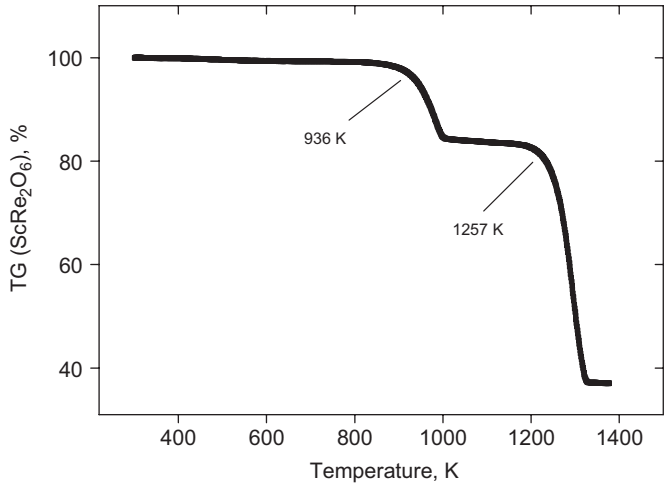

Fig. 2. Thermal decomposition of $ScRe_2O_6$ in Ar-atmosphere with a rate of heating of 5 K/min.

3.2. High-pressure high-temperature synthesis

The formation of $ScRe_2O_6$ crystals is observed after synthesis under high pressure of 5 GPa and a temperature of 1573 K. According to X-ray diffraction, the sample with nominal composition "$Sc_2Re_3O_{12}$" contained after the synthesis about 78 wt% of $ScRe_2O_6$, 22 wt% of Sc_6ReO_{12} and traces of $Sc(ReO_4)_3 \cdot 3H_2O$. The presence of water molecules in scandium perrhenate is due to X-ray measuring of the sample in air during some hours: it is known that the most of perrhenates of two- and three-valent metals are stable in air only in the form of hydrates. All reflections, which do not belong to Sc_6ReO_{12} and scandium perrhenate hydrate, were explained based on a monoclinic unit cell with lattice parameters $a = 5.6140(2)$ Å, $b = 4.7951(1)$ Å, $c = 7.5048(3)$ Å and $\beta = 97.483(2)^\circ$.

3.3. Crystal structure of $ScRe_2O_6$

The crystal structure of $ScRe_2O_6$ was first solved by a combination of X-ray powder and electron diffraction. From selected area, electron diffraction (SAED) patterns a monoclinic unit cell with $a = 5.65$ Å, $b = 4.78$ Å, $c = 7.61$ Å and $\beta = 97.7^\circ$ was determined. A group of strong reflections forms a subcell with $a = b = 4.78$ Å, $c = 2.95$ Å, $\alpha = \beta = \gamma = 90^\circ$. This tetragonal pseudo symmetry and the close relation of the unit cell $\{\mathbf{a},\mathbf{b},\mathbf{c}\}$ with an ideal rutile unit cell $\{\mathbf{a}_t,\mathbf{b}_t,\mathbf{c}_t\}$, $\mathbf{a} = -\mathbf{b}_t + \mathbf{c}_t$, $\mathbf{b} = \mathbf{a}_t$, $\mathbf{c} = \mathbf{b}_t + 2\mathbf{c}_t$, suggest to derive a start model from the rutile structure. The extinction rules are in agreement with space group $P2_1/a$. With a shift of the origin by $1/2\mathbf{c}_t$, the cation positions in the three-fold superstructure cell are situated on the (2*b*) site at $(0, \frac{1}{2}, \frac{1}{2})$ and on a (4*e*) site (x_c, y_c, z_c) with $x_c \approx 1/6$, $y_c \approx 0$, $z_c \approx 1/6$. The 12 oxygen ions are transformed onto three (4*e*) sites with $x_1 \approx (3–4x)/6$, $y_1 \approx x$, $z_1 \approx (3+2x)/6$, $x_2 \approx (1+4x)/6$, $y_2 \approx 1-x$, $z_2 \approx (1–2x)/6$, and $x_3 \approx (7–4x)/6$, $y_3 \approx x$, $z_3 \approx (1+2x)/6$, respectively, were x refers to the oxygen site in rutile $(x, x, 0)$ with $x \approx 0.30478(6)$ in TiO_2 [17]. This initial model was refined for different assumptions for the occupation of the (2*b*) and (4*e*) cation sites by the Rietveld method. The structure model converged rapidly for Sc on the (2*b*) and Re on the (4*e*) site. This model was later confirmed by single crystal X-ray diffraction performed on crystals, which were obtained by the high-pressure high-temperature synthesis (Tables 1–3). An anisotropic Lorentzian contribution

Table 1
Details of X-ray single-crystal data collection and structure refinement of $ScRe_2O_6$

Chemical formula	$ScRe_2O_6$
Formula weight	513.36
Crystal system	Monoclinic
Space group	$P2_1/a$ (no. 14)
Unit cell dimensions	$a = 5.6176(9)$ Å $b = 4.7970(9)$ Å $c = 7.5143(16)$ Å $\beta = 97.49(2)^\circ$
Cell volume (Å^3)	200.76(7)
Z	2
Calculated density (g/cm^3)	8.492
Radiation type	Mo–$K\alpha$, $\lambda = 0.71073$ Å
No. of reflections for cell parameters	836
d range for cell determination (Å)	0.7556–7.498
Temperature (K)	293(2)
Crystal form, color	Prismatic, black
Crystal size (mm^3)	$0.028 \times 0.020 \times 0.015$
Data collection	
Diffractometer	Oxford Diffraction Xcalibur, single-crystal X-ray diffractometer with sapphire CCD detector
Data collection method	Rotation method data acquisition using ω and φ scans (s)
Absorption coefficient	61.719 mm^{-1}
$F(0\,0\,0)$	438
Theta range for data collection	5.05–27.59 °
Range of h, k, l	$-7 \leqslant h \leqslant 4$, $-5 \leqslant k \leqslant 6$, $-8 \leqslant l \leqslant 9$
Reflections collected/unique	1054/300
Completeness to $\theta = 27.59^\circ$	0.645
Refinement method	Full-matrix least-squares on F^2
Data/restraints/parameters	300/0/18
Goodness-of-fit on F^2	1.310
Final R indices [$I > 2\sigma(I)$]	$R_1 = 0.0529$, $wR_2 = 0.0955$
R indices (all data)	$R_1 = 0.0683$, $wR_2 = 0.1035$
Largest diff. peak and hole	3.571−3.102 e/Å^3

Table 2
Atomic coordinates and equivalent isotropic displacement parameters (Å^2) for $ScRe_2O_6$

Atom	Site	x	y	z	Occup.	U(eq)
Sc	2*a*	0	0.5	0.5	1	0.000(2)
Re	4*e*	0.1283(3)	0.0087(2)	0.1507(2)	1	0.001(1)
O	4*e*	0.168(4)	0.826(4)	0.378(3)	1	0.010(5)
O	4*e*	0.4180(4)	0.216(4)	0.247(3)	1	0.010(4)
O	4*e*	0.3380(4)	−0.270(5)	0.067(3)	1	0.012(5)

Table 3
Selected interatomic distances (Å) and angles (°) for $ScRe_2O_6$

Re–O(1)	1.91(2)	O(4)–Re–O(3)	82.3(9)
Re–O(2)	1.97(2)	O(2)–Re–O(4)	90.9(8)
Re–O(2)	1.96(2)	O(4)–Re–O(4)	90.4(4)
Re–O(3)	1.94(2)	O(3)–Re–O(4)	89.8(8)
Re–O(3)	1.98(2)	O(4)–Re–O(4)	101.9(8)
Re–O(3)	2.03(2)	O(3)–Re–O(4)	175.3(7)
Sc–O(1)	2.10(2) (*x*2)	O(2)–Re–O(3)	84.8(9)
Sc–O(1)	2.14(2) (*x*2)	O(4)–Re–O(3)	87.7(8)
Sc–O(2)	2.16(2) (*x*2)	O(3)–Re–O(3)	92.0(5)
Re–Re	2.523(3)	O(2)–Sc–O(2)	180.0(7) (*x*2)
Sc–Re	3.134 (2)	O(2)–Sc–O(2)	86.5(5) (*x*2)
O(2)–Re–O(4)	88.3(8)	O(2)–Sc–O(2)	93.5(5) (*x*2)
O(2)–Re–O(3)	89.2(7)	O(2)–Sc–O(3)	91.7(6) (*x*2)
O(4)–Re–O(3)	177.5(7)	O(2)–Sc–O(3)	74.7(9) (*x*2)
O(2)–Re–O(4)	166.8(7)	O(2)–Sc–O(3)	105.3(9) (*x*2)
O(4)–Re–O(4)	88.5(5)	O(2)–Sc–O(3)	88.3(6) (*x*2)
O(3)–Re–O(4)	93.9(7)	O(3)–Sc–O(3)	180.000(1)

to particle size broadening of reflections was taken into account during Rietveld refinement by the "LorSiz" parameter in *FullProf* for the platelet–needle vector along $[\bar{1}\,1\,1]$.

The crystal structure of $ScRe_2O_6$ is presented in Fig. 3a, demonstrating the analogy with the rutile structure. All studied crystals were reticular meroedric twins, which could indicate a structural phase transition from $ScRe_2O_6$ with a higher symmetry formed at high-pressure and high-temperature conditions, to one with rutile-like structure, stable under ambient conditions. Due to strong overlaps of reflections of both domains, the completeness to $\theta = 27.59^\circ$ was only 64.5% (Table 1) and only isotropic thermal displacement parameters for all sites could be determined (Table 2).

The structure of $ScRe_2O_6$ can formally be considered as consisting of Sc-layers, which are separated from each other by Re_2O_6-layers (Fig. 3b and c). The coordination polyhedra of Sc are octahedra, which are connected with each other via corners and with ReO_6-octahedra via edges. ScO_6 octahedra are nearly regular having the smallest Sc–O distance of 2.10(2) Å and the largest one of 2.16(2) Å (Table 3). The average Sc–O distance (2.13 Å) is in good agreement with this value for ScO_6-octahedra (2.12 Å) in Sc_2O_3 [18]. ReO_6-octahedra form units consisting of two octahedra connected via edges with a Re–Re distance of 2.523(3) Å (Table 3). This distance is considerably shorter than in metallic rhenium (2.74 Å) and, therefore, is interpreted as a metallic bond. ReO_6-octahedra from neighboring chains are corner-sharing with the shortest Re–Re distance from neighboring chains of 3.641(3) Å. Re–O distances in the ReO_6-octahedron range from 1.91(2) to 2.03(2) Å.

In the Inorganic Crystal Structure Database (ICSD) [19] we have not found any other compound, which adopts the $ScRe_2O_6$ structure with analogous parameters. $SbRe_2O_6$ (S.G. *C*2/*c*) [20] and $BiRe_2O_6$ (S.G. *C*2/*m*) [21] show the closest structural relationship with $ScRe_2O_6$. The comparison of the $ScRe_2O_6$ and $SbRe_2O_6$ structures is more appropriate due to the similar ionic radii of Sc^{3+} and Sb^{3+} [22]. All three structures consist of alternating layers of Re atoms, which are octahedrally coordinated by oxygen atoms and form Re_2O_{10} clusters with Re–Re metallic bonds with a length of 2.517(1) Å ($SbRe_2O_6$) and 2.508(1) Å ($BiRe_2O_6$). The Re,O-layers in the $SbRe_2O_6$ structure are also separated by Sb atoms as the corresponding ones by Sc atoms in $ScRe_2O_6$. However, Sb atoms lie in a different direction with respect to the close-packed oxygen lattice in comparison with Sc in the $ScRe_2O_6$ structure, so that a similarity to the rutile structure is only detected for the $[Re_2O_6]_n$-fragment. Moreover, the Sb atoms are four-fold coordinated by oxygen atoms. In spite of the same ionic radius of Sc^{3+} and Sb^{3+}, the average distance between Re_2O_6-layers in $SbRe_2O_6$ is about 0.2 Å longer than the corresponding value in $ScRe_2O_6$ due to the lone-electron pair of Sb^{3+}. In $BiRe_2O_6$, bismuth atoms occupy different sites with two coordination polyhedra: one is similar to that of Sb in $SbRe_2O_6$ and the other is a distorted octahedron.

Due to a layer-type structure, an anisotropy of physical properties of $ScRe_2O_6$ such as magnetism and electrical conductivity along [0 1 0] and [0 0 1] directions could be expected.

The high-temperature structural behavior of $ScRe_2O_6$ was investigated in the temperature range of 295–930 K by means of synchrotron powder diffraction. No phase transition was found in this temperature interval. The dependence of relative changes of lattice parameters on temperature, normalized to the values at 295 K, is presented in Fig. 4. Thermal expansion of $ScRe_2O_6$ is nearly isotropic with an average coefficient of expansion along the "*a*" axis about $4.6 \times 10^{-6}\,K^{-1}$, along the "*b*" axis about $3.5 \times 10^{-6}\,K^{-1}$ and along the "*c*" axis about $5.3 \times 10^{-6}\,K^{-1}$. The monoclinic angle becomes smaller with increasing temperature. The Re–Re distance increases slightly with temperature and is only 1.5% longer at 930 K than at room temperature, so that no indication for a break of the metallic Re–Re bonds is observed.

3.4. Magnetization and resistivity measurements on $ScRe_2O_6$

Sc^{3+} ions are diamagnetic and, therefore, the magnetic properties of $ScRe_2O_6$ are determined by the electronic configuration of the Re-ions. The temperature dependence of magnetization in a constant magnetic field of 1 T, shown in Fig. 5, demonstrates a nearly temperature-independent paramagnetism between 40 and 350 K with a magnetization value of $1.38 \times 10^{-3}\,\mu_B$/f.u. or $6.9 \times 10^{-4}\,\mu_B$/Re-ion at 293 K. No differences between ZFC (zero-field cooling mode) and FC (field-cooling mode) data were detected at this high field strength. The field dependences of magnetization at 10, 50, 100, 150, 300 and 330 K show hysteresis

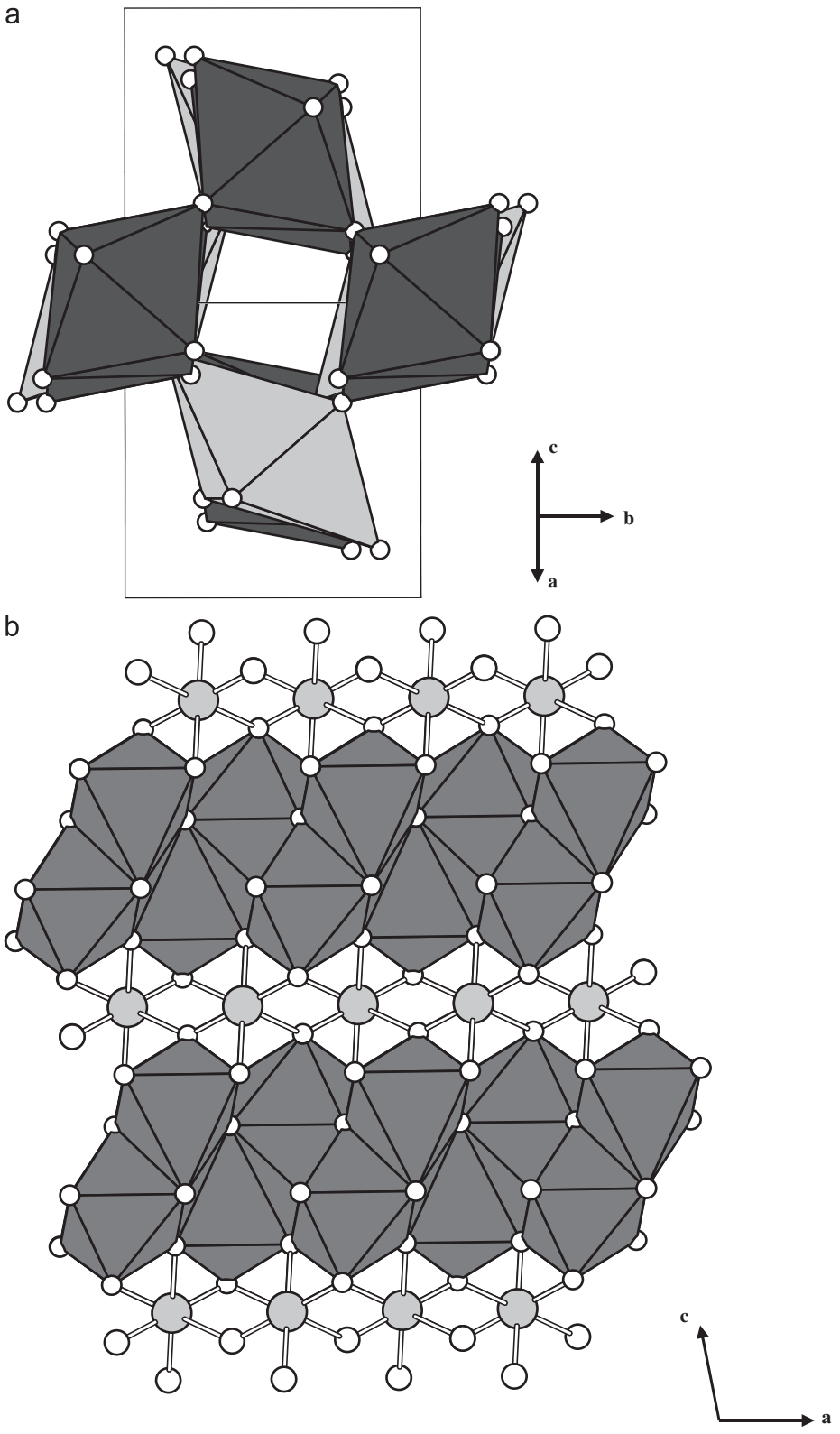

Fig. 3. (a) The crystal structure of $ScRe_2O_6$ viewed towards the (1 0 2) plane, demonstrating the analogy with the rutile structure [17]. Dark gray octahedra are ReO_6, light gray ones are ScO_6. (b) The crystal structure of $ScRe_2O_6$ in the ac-plane showing the $[Re_2O_6]_n$ layers separated by Sc layers. Small white spheres are O^{2-} ions, large light gray ones are Sc^{3+} ions. ReO_6 octahedra are connected via edges and corners.

effects (Fig. 6), which indicate ferromagnetic ordering in $ScRe_2O_6$ at least in the investigated temperature range from 10 to 330 K. After annealing of the sample at 1473 K during 24 h in Ar-atmosphere only diamagnetic signals were registered, which correspond to the Sc_2O_3 phase as identified by X-ray diffraction.

Resistivity measurements in the temperature range of 4–270 K revealed a metallic type of conductivity in $ScRe_2O_6$ (inset in Fig. 5) with specific resistivities of $4.5(4)\times10^{-6}\,\Omega\,m$ at 4 K and $8.2(7)\times10^{-6}\,\Omega\,m$ at 270 K. Additional high-temperature data from another instrument and specimen confirmed qualitatively also a metallic behavior up to 950 K. Note that the temperature dependence of resistivity does not obey the behavior of a Fermi liquid, $\rho(T)=\rho_0+AT^2$, but a cross-over between two regions (up to 30 K and above 100 K) with linear increases of resistivity and different slopes.

A metallic character of conductivity was also observed for single crystals of $SbRe_2O_6$ along the $[Re_2O_6]_n$-layers with $R=6.1\times10^{-7}\,\Omega\,m$ at room temperature [20]. In order to determine the number of conducting electrons per formula unit by Hall measurements, larger single crystals of $ScRe_2O_6$ than available now are required.

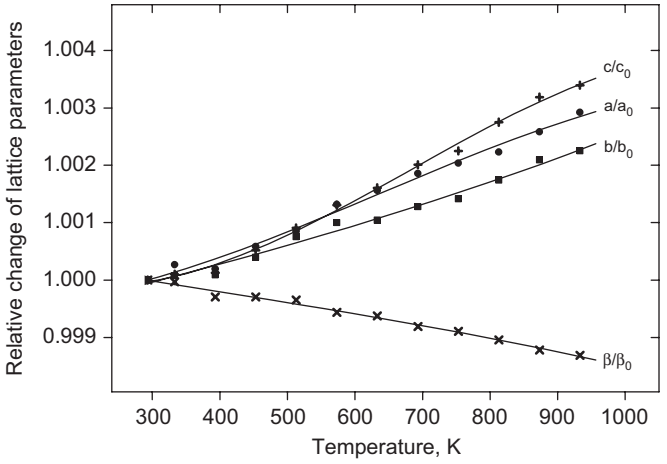

Fig. 4. Relative changes of lattice parameters for $ScRe_2O_6$, normalized to the values at 295 K.

4. Discussion

$ScRe_2O_6$ is the first example of a Sc-containing ternary oxide with a 5*d*-cation crystallizing in a rutile-like structure like other ternary oxides of 3*d* elements and Re, such as Cr, Fe, Co or Ni [23]. Our preliminary results [24] have shown, for example, that in the system Cr–Re–O, a compound $(Cr_{1/3}Re_{2/3})O_2$ with rutile-structure and a random distribution of Cr and Re cations on one site exists. In this case, the sizes of Cr and Re cations are similar. The cation sizes are sufficiently different between Sc^{3+} (0.75 Å) and Re^{+4} (0.63 Å) or Re^{+5} (0.58 Å), and cation order results in the structure of $ScRe_2O_6$. Note that the observed splitting of the cation site in $ScRe_2O_6$ with respect to the rutile aristotype is essentially different to the one in the trirutile superstructure.

A survey of Re in oxides with metallic Re–Re bonds such as compounds in the system *Ln*–Re–O (*Ln*-rare earth element [25–28]), orthorhombic [29] and monoclinic [30] modifications of ReO_2, $SbRe_2O_6$ [20] and $BiRe_2O_6$ [21] revealed no unambiguous correlation between Re–Re distance and formal Re–Re bond order, calculated from the oxidation state of rhenium. This means that not necessarily all electrons of Re, which are not involved in Re–O bonds, participate in the metallic Re–Re bond, but some electrons could be delocalized instead, which must be reflected in the transport properties of the compound. For example, the Re–Re distance in monoclinic ReO_2 is 2.49 Å with a formal bond order of 3 and metallic character of conductivity, while the Re–Re distance in semiconducting Eu_2ReO_5 with the same metallic bond order is 2.256 Å [27],

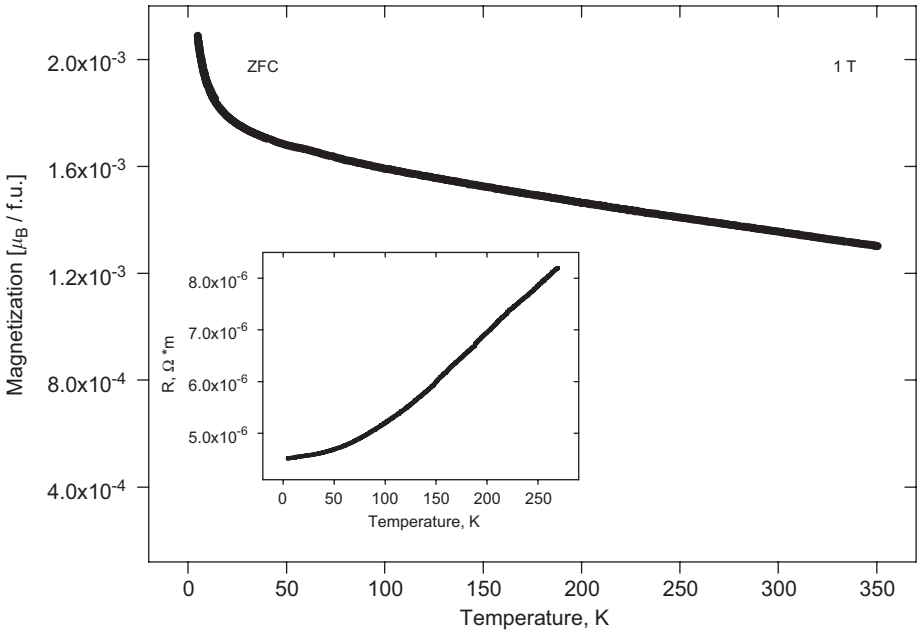

Fig. 5. Temperature dependence of magnetization, measured at the field strength of 1 T, and resistivity (inset) for $ScRe_2O_6$.

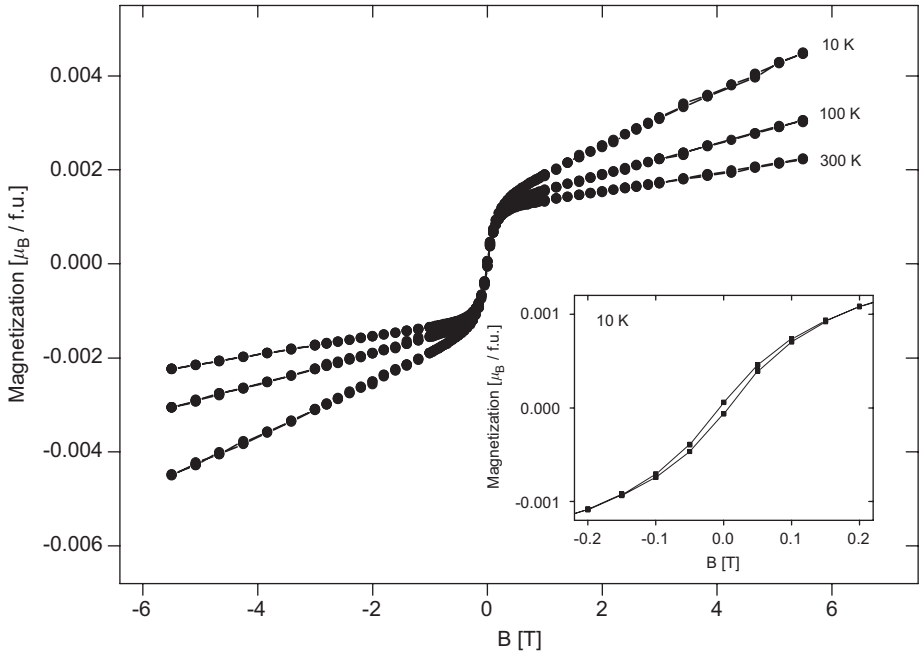

Fig. 6. Hysteresis loops of $ScRe_2O_6$ at 10, 100 and 300 K. The linear high-field behavior indicates that only a small component of the magnetic moments is ferromagnetically aligned.

indicating a higher multiplicity of the Re–Re bond in the latter one.

The similarity of the Re–Re bond length (2.52 Å) for $ScRe_2O_6$, $SbRe_2O_6$ and $BiRe_2O_6$ with Re +4.5 and similar conductivities (for $ScRe_2O_6$ and $SbRe_2O_6$) suggest the same Re–Re bond order in these compounds and, therefore, the same number of conducting electrons. Note that $Tm_5Re_2O_{12}$ [25], $Dy_5Re_2O_{12}$ and $Ho_5Re_2O_{12}$ [28] with the same average oxidation state of Re +4.5 form a shorter Re–Re bond of about 2.44 Å. Unfortunately, their transport properties were not investigated. The formation of metallic Re–Re pairs in $Ln_5Re_2O_{12}$ (Ln = Tm, Dy and Ho) was proposed to result from the Peierls instability of a one-dimensional metallic chain [31]. $ScRe_2O_6$ and $SbRe_2O_6$ are examples, where some of the electrons form metallic Re–Re bonds like in the dimerized Peierls ground-state, while other electrons remain delocalized resulting in metallic conductivity. However, in $ScRe_2O_6$ and $SbRe_2O_6$ the Re–Re pairs form one-dimensional chains in contrast to the Peierls ground state, where a one-dimensional chain breaks down into pairs.

Ternary oxides with metallic Re–Re bonds and no other ions with a permanent magnetic moment demonstrate either Curie–Weiss behavior and semiconducting properties such as $La_3Re_2O_{10}$ [32] or temperature independent Pauli-paramagnetism of conducting electrons and metallic conductivity such as $Ln_4Re_6O_{19}$ [33]. $ScRe_2O_6$ is the first example of a metallic complex oxide with Re–Re bonds showing ferromagnetic ordering above room temperature. A ferromagnetic component above room temperature was already observed for some Sr–Re-oxides without Re–Re bonds and Re in an oxidation state lower than +7, for instance for $Sr_{11}Re_4O_{24}$ [34] and $Sr_7Re_4O_{19}$ [35]. In the structure of $Sr_7Re_4O_{19}$, there is also a two-dimensional system of infinite chains of ReO_6-octahedra linked together by common corners, and each chain is connected with another one via the corners of each second ReO_6-octahedron. A T_c above room temperature was also registered for this compound, but nothing is known about the electronic conductivity and the magnetic coupling mechanism. A strong correlation between electronic transport behavior and magnetic coupling is proposed. Further investigations by Hall measurements and studies of magnetoresistance are essential to elucidate this "unconventional Re-magnetism", i.e. the surprisingly high magnetic ordering temperatures in $ScRe_2O_6$ and some other ternary Re-containing oxides. Calculations of the spin-polarized band structure are necessary to reveal the underlying mechanism.

Acknowledgments

Financial support from the *Deutsche Forschungsgemeinschaft* (DFG FU125/42) is gratefully acknowledged. The authors are indebted to T. Kautz (Institut für Geowissenschaften, Johann Wolfgang Goethe Universität Frankfurt am Main, Germany) for assistance in performing the high-pressure high-temperature synthesis, to Dr. H. Höfer (Institut für Geowissenschaften, Johann Wolfgang Goethe Universität Frankfurt am Main, Germany) for performing the EPMA measurements.

Appendix A. Supplementary materials

Supplementary data associated with this article can be found in the online version at doi:10.1016/j.jssc.2007.11.021.

References

[1] D. Michel, A. Kahn, M. Perezyjorba, Mat. Res. Bull. 11 (7) (1976) 857–865.
[2] L.N. Komissarova, Inorganic and Analytical Chemistry of Scandium, Editorial URSS, Moscow, 2001 (in Russian).
[3] J.A. Valdez, M. Tang, K.E. Sickafus, Nucl. Instr. and Meth. B 250 (2006) 148–154.
[4] Y. Yokogawa, M. Yoshimura, J. Am. Ceram. Soc. 82 (6) (1999) 1585–1588.
[5] W.L. Zhong, P.L. Zhang, H.C. Chen, Sol. State Commun. 49 (5) (1984) 467–469.
[6] D. Mikhailova, H. Ehrenberg, H. Fuess, J. Solid State Chem. 179 (2006) 3672–3680.
[7] V.A. Gagarina, V.V. Fomichev, L.Z. Gokhman, K.I. Petrov, Russ. J. Inorg. Chem. 22 (N7) (1977) 1832–1835 (Engl. Transl.).
[8] T. Hartmann, H. Ehrenberg, G. Miehe, G. Wltschek, H. Fuess, J. Solid State Chem. 148 (1999) 220–223.
[9] L.N. Komissarova, M.B. Varfolomeev, V.I. Ivanov, V.E. Plyutshev, Doklady Akademii Nauk 160 (3) (1965) 608–611 (in Russian).
[10] V.N. Khrustalev, M.B. Varfolomeev, Yu.T. Struchkov, Russ. J. Inorg. Chem. 42 (1997) 1779–1784 (Engl. Transl.).
[11] T. Roisnel, J. Rodriguez-Carvajal, Mater. Sci. Forum 378–381 (2001) 118–123.
[12] G.M. Sheldrick, Acta Crystallogr. A 46 (1990) 467–473.
[13] G.M. Sheldrick, SHELXL97, Program for the Refinement of Crystal Structures, University of Göttingen, Germany, 1997.
[14] Stoe & Cie, X-STEP32, 2000, Stoe & Cie GmbH, Darmstadt, Germany.
[15] CrysalisRed, CCD data reduction GUI, version 1.171.26, Oxford Diffraction Poland, 2005.
[16] G. Miehe, Thesis, Report on 3rd DGK, Darmstadt, Germany, 1995, p. 51.
[17] C.J. Howard, T.M. Sabine, F. Dickson, Acta Cryst. B 47 (1991) 462–468.
[18] T. Schleid, G. Meyer, J. Less-Common Met. 149 (1989) 73–80.
[19] Inorganic Crystal Structure Database (ICSD), Fachinformationszentrum Karlsruhe, Germany, 2006.
[20] H. Watanabe, H. Imoto, H. Tanaka, J. Solid State Chem. 138 (1998) 245–249.
[21] A.R. Rae Smith, A.K. Cheetham, J. Solid State Chem. 30 (1979) 345–352.
[22] R.D. Shannon, Acta Crystallogr. A 32 (1976) 751–767.
[23] A.W. Sleight, Inorg. Chem. 14 (3) (1975) 597–598.
[24] D. Mikhailova, in preparation.
[25] H. Ehrenberg, T. Hartmann, G. Wltschek, H. Fuess, W. Morgenroth, H.-G. Krane, Acta Cryst. B 55 (1999) 849–852.
[26] W. Jeitschko, D.H. Heumannskämper, M.S. Schriewer-Pöttgen, U.Ch. Rodewald, J. Solid State Chem. 147 (1999) 218–228.
[27] C. Mujica, D. Gutiérrez, J. Llanos, R. Cardoso, J. Alloys Compd. 307 (2000) 127–130.
[28] H. Ehrenberg, T. Hartmann, K.G. Bramnik, G. Miehe, H. Fuess, Solid State Sci. 6 (2004) 247–250.
[29] D.B. Rogers, R.D. Shannon, A.W. Sleight, J.L. Gillson, Inorg. Chem. 8 (1969) 841–849.
[30] H.P.S. Correa, I.P. Cavalcante, L.G. Martinez, C.G.P. Orlando, M.T.D. Orlando, Braz. J. Phys. 34 (2004) 1208–1210.
[31] H. Ehrenberg, T. Hartmann, G. Wltschek, R. Doyle, H. Fuess, Mater. Struct. Chem. Biol. Phys. Tech. 5 (1998) 82.
[32] C.C. Torardi, A.W. Sleight, J. Less-Common Met. 116 (1986) 293–299.
[33] A. Sasaki, M. Wakeshima, Y. Hinatsu, J. Phys.: Condens. Matter 18 (2006) 9031–9046.
[34] K.G. Bramnik, G. Miehe, H. Ehrenberg, H. Fuess, A.M. Abakumov, R.V. Shpanchenko, V.Yu. Pomjakushin, A.M. Balagurov, J. Solid State Chem. 149 (2000) 49–55.
[35] K.G. Bramnik, H. Ehrenberg, H. Fuess, J. Solid State Chem. 160 (2001) 45–49.